INTERNATIONAL JOURNAL OF ADVANCE RESEARCH, IDEAS AND INNOVATIONS IN TECHNOLOGY

ISSN: 2454-132X
Impact factor: 6.078
(Volume 6, Issue 2)
Available online at: www.ijariit.com

Numerical investigation of a modified NACA-0018 Airfoil using Bumpy Profile at Low Reynolds Number

Ammar Ewis
amarewes@gmail.com
The British University in Egypt, Cairo, Egypt

Ahmed El-Baz
ahmed.elbaz@bue.edu.eg
The British University in Egypt, Cairo, Egypt

ABSTRACT

Flow separation is one of the major problems affecting the performance of all airfoils under high angle of attack. Several passive flow mechanisms have been investigated to limit this phenomenon and improve the aerodynamic efficiency of the airfoil by increasing the lift force while decreasing the drag force associated with it. This study investigates the application of surface bumps over both the suction and pressure sides of the NACA-0018 airfoil at low Reynolds number of 500,000. The bump shapes resemble the shape of the Hawk which does not show smooth profile in nature. The bumps are introduced in the form of sine waves with different amplitudes and periods. Bumps on each side have been investigated separately, the optimum amplitude and period are determined, the two optimum parameters were joined together forming a new airfoil shape. It was found that this approach limits separation at the stall angle and reduces the drag force as a result of the bumps on the suction side. The bumps on the pressure side were found to enhance the lift force as high-pressure spots are formed, which increase the differential pressure. Glide ratio improvement of 17% was reached using the modified airfoil.

Keywords— *CFD, bio-inspired, airfoils, Hawk wing*

1. INTRODUCTION

Humans have so many things to learn from mother nature. Commonly, the naturally available designs show a superior performance than those produced by a human. When humankind try to copy nature, this often results in a poorer version with inferior performance than that of the natural design. In our current global crisis of global warming, it is believed nature will continue its rule in inspiring humans to reach a new solution to save Planet Earth. One of nature's main inspiration is the living creatures such as birds, whales, flies, and all other flying creatures.

Design of an airfoil is an empirical procedure based on experiments rather than solid science, as time passed, and humans gained more experience with various airfoils it was always assumed that the streamlined shape offers the best performance in terms of high lift and low drag. Ju and Zang (2012) stated that the optimum airfoil for a wind turbine must have a high glide ratio, high lift and low sensitivity to roughness on the leading edge. However, one of the main parameters affecting the performance of the airfoil is the flow separation that takes place under high angle of attacks. The detachment of air from the surface of the airfoil causes an increase in the generated drag force and a drop of the lift as a result of the generated vortices on the suction side of the airfoil. Different flow control mechanisms both active and passive were investigated previously to mitigate the separation problem and increase the glide ratio.

Bio-inspired airfoil shapes have been reported to improve the aerodynamic performance by many researchers. The dragonfly wing was researched from the early days, Rees et al (1975) were the first to study the dragonfly corrugations suggesting that it only improves flow characteristics but not the lift. Almost all recent studies agree that the corrugated shape offers superior aerodynamic performance, but the explanation of such phenomena varies from one study to the other. The first hypothesis states that the air is trapped inside the corrugations in a stagnant or slow rotation pattern causing the wing to act as streamed airfoil, Reec et al (1975). The second hypothesis is more concerned with the flow reattachment, as the incoming airflow angle of attack increase triggers the separation phenomena, the corrugations in the airfoil cause flow reattachment sooner than the streamlined airfoil. In the latter case, a large recirculation bubble is formed, which leads to collapse of lift. The presence of surface corrugations, on the other hand, maintains the lift force generated on the corrugated airfoil (B.G. Newman, 1977). The second hypothesis was then further explained by Kessel (2000), as he measured the pressure on the suction side and found that negative pressure regions were found at the groves of the dragonfly wing model. The presence of the negative pressure vortices was then confirmed via several numerical studies, (Mittal A. V., 2004), (M.Sun, 2005) and (R.Mittal, 2005).

© 2020, www.IJARIIT.com All Rights Reserved

Investigations of the lift and drag coefficients of the dragonfly wing done by various studies revealed that at low Reynold's number the corrugated airfoil showed better aerodynamic characteristic by delaying the separation and enhancing the lift force, while at higher Reynold's number it was concluded that the profiled airfoil is better. Kessel (2000) found that at zero angle of attack the lift force was highest for the flat plate and lowest on the profiled airfoil, this is not making sense as at zero angles of attack the profiled airfoil should yield the largest lift compared to the flat plate, so this study was disregarded from the analysis of the forces. Mittal and Vargas (2004) studied the different types of drag, it was found that for the corrugated airfoil shear drag only contributed by ¼ of the total drag, on the other hand, it contributes by 2/3 of the total drag for the plate and profiled shapes. This can explain why the enhancements in the aerodynamic characteristics offered by the corrugated airfoil are only present at low Reynold's numbers where the shear drag is minimum. Another study investigated the lift and drag between the profiled airfoil, flat plate and corrugated airfoil New (2014). The corrugated airfoil showed an enhancement of 25% at low Reynold's number of 58,000. On the other hand, increasing Reynold's number to 125,000 showed that the profiled airfoil is better performing.

The Humpback whale fin profile is also a popular form of biomimetics. A study was done at the Canadian Naval academy (Hamiltn, 2008) using modified airfoils with leading edge tubercles similar to a humpback whale fin, the stall was delayed from 12 degrees to 18 degrees. In that study, the lift force showed an increase of 8% while the drag force was reduced by 32%. Another experimental study using leading edge tubercles (Miklosovic, 2004), done on NACA0020 airfoil at Reynold's number of $5x10^5$, showed that below the stall angle there is no improvement, while stall is delayed significantly. A study done by Tze et al (2015), investigated the effect of changing the wavelength and amplitude of the leading-edge undulations. The study was performed on NACA65-(12)10 at Reynold's number of 150,000. The results showed that increasing the frequency causes a positive impact while increasing the amplitude showed a negative impact. This was found even though the separation decreased but the lift generating surface area also decreased, thus decreasing the lift.

The mechanism that the leading-edge undulations work is controversial. The first hypothesis (E. van Nierop, 2008) (H. Johari, 2007) stated that the pressure distribution change over the airfoil, this delays the separation behind the undulation. As now the airfoil has a different chord length, but the same thickness then similar pressure must be overcome but under the condition of shorter distance, which delay the separation. Van Nierop (2008) and Johari (2007) also suggested that stall transition will be smoother, some parts of the airfoil will undergo separation while the flow over other parts will stay attached, this causes the peak lift to be decreased but maintains a suitable lift over larger flow angles. Another hypothesis (Stanway, 2008) (K. L. Hansen, 2011), suggested that the reason behind the delay in separation is due to the formation of a structured vortex. As the leading-edge undulations act as vortex generators two counter-rotating vortexes are formed in the gap between the undulations, the strength of the vortex increases with the increase in the angle of attack. The vortex creates a suction force that induces the lift generating mechanism, the lift produced as a result of the vortices is smaller than that generated due to the pressure hence maximum lift is never achieved

The concept of introducing bumps to the surface was first discussed in NACA reports as far as 1932 (Jacobs E. , 1932) (Jacobs E. , 1932) by Jacobs. It was found that using 4 bumps with a height of 0.2%C reduced the drag force and decreased the separation. More recently Lyon et al (1997) also confirmed the drag reduction phenomena associated with surface bumps. They used a trip layer on the surface of an airfoil which acted as the bumps. They reported a reduction in the drag force. Another research at NASA Langley research center (Owens W. E., 2005) confirmed the drag reduction effect by 12-15% after introducing contour bumps close to the trailing edge.

The delay in separation when surface bumps are used was proven by Arvind et al (2012). The flow was visualized by the aid of smoke wire and improvements in the flow characteristics and reattachment were shown clearly under Reynolds numbers of 25,000 and 50,000. The delay in separation together with improvement in the aerodynamic characteristics was also reported by Asif et al (2018). In their investigation of E398 airfoil with a uni-bump of height 0.9%C, it was found that at Reynolds number of 36,000, the location of the bump was found to be optimum closer to the leading edge of the airfoil. As the bump moved towards the maximum thickness point, flow separation was delayed from 46%C to 56%C at an angle of attack of 11degrees. The lift force increased while drag reduction was only reported at high angle of attack. The peak performance was found when the bump was located at 10%C from the leading edge.

The previous survey of literature show that airfoils with continuous bumpy surfaces have not been investigated thoroughly. Therefore, a systematic numerical investigation of the effect of continuous sinusoidal waves on the suction side, the pressure side, or both sides of an airfoil is performed. The NACA0018 airfoil is selected due to its wide applicability in vertical axis wind turbines. The continuous bumpy shape is inspired by the Hawk's wing shape formed by layers of feathered structure. The bumpy airfoil surface approach was adopted to reflect a more refined and smoother transition between bumps as seen in the Hawk's wing. The bumps are applied to the airfoil surface by developing a polynomial approximation describing the surface of the airfoil and super positioning a sine wave on it. The amplitude and period of the sine wave was be varied to obtain the optimum combination for both the suction side and the pressure side of the airfoil. Both quantitative and qualitative analyses are presented for the flow characteristics over the airfoil. Quantitative analysis using the lift and drag coefficients as well as the glide ratio are presented for the original airfoil shape and the modified shapes. This is appended by studying the variation of the pressure coefficient along both sides of the airfoil for each geometry. Qualitative analysis includes the velocity and pressure contours together with the flow streamlines for the different configurations of the surface bumps.

2. AIRFOIL GEOMETRY AND SURFACE BUMPS

The NACA0018 airfoil coordinated were obtained using airfoil tools (Airfoil tools, 2020). A sixth-order polynomial was generated to represent the airfoil shape, equation 1. Figure 1 shows a comparison between the original shape and the approximate polynomial.

$$Y/C = -6.256(X/C)^6 + 22.03(X/C)^5 - 28.505(X/C)^4 + 18.308(X/C)^3 - 6.299(X/C)^2 + 1.1109(X/C) + 0.0093 \quad (1)$$

© 2020, www.IJARIIT.com All Rights Reserved

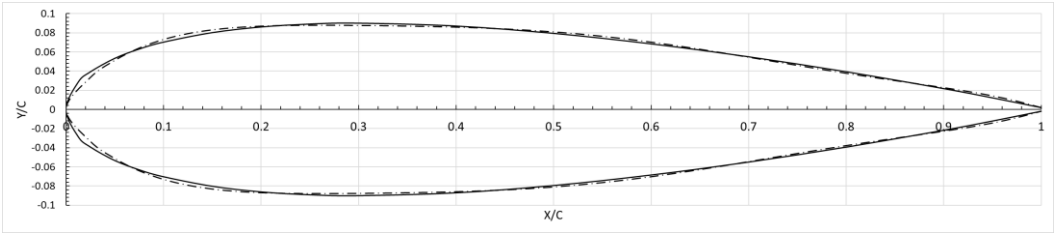

Fig. 1: Airfoil polynomial approximation, solid line airfoil tools and dotted line polynomial approximation (Airfoil tools, 2020)

The surface bumps are represented by sine wave equation super positioned on the airfoil surface. The general sine wave equation, equation 2, is used to provide the bump height (Y_b/C) in terms of the wave amplitude (A_b/C), the X coordinate (X/C) and the bump wave period (T_b/C). Different amplitudes and periods of the wave were implemented. Tables 1 and 2 show the values of A_b and T_b examined in the present investigation.

Table 1: Investigated Combinations for suction side

Configuration#	**1**	**2**	**3**	**4**	**5**
A_b/C (%)	0.2	0.3	0.4	0.3	0.3
T_b/C (%)	25	25	25	15	35

Table 2: Investigated Combinations for pressure side

Configuration#	**1**	**2**	**3**	**4**	**5**
A_b/C (%)	0.3	0.4	0.5	0.4	0.4
T_b/C (%)	25	25	25	15	10

$$\frac{Y_b}{C} = A_b \mathrm{Sin}\left(\frac{2\pi x}{T}\right) \tag{2}$$

3. NUMERICAL METHODOLOGY AND VALIDATION

The numerical study was made using a C-domain, Figure 2. The airfoil is located at the origin while the inlet boundary is formed by a semi-circle of radius 15 C. The cross-stream domain width is 30 C while the downs stream length of the domain is 40 C. These domain dimensions ensure domain independent results (Gasser E. Hassan, 2014). The boundary condition on the domain sides are symmetry boundary conditions while the downstream boundary is outlet.

The numerical solution of the Reynolds Averaged Navier Stokes equations was obtained using ANSYS-FLUENT software. Turbulence was solved using the two equations realizable $k-\varepsilon$ model. Pressure-velocity coupling SIMPLE algorithm was used. Discretization of convection terms was made using the second order upwind scheme. Iterative solution was adopted with residuals less than 10^{-6}. The angle of attack of the airfoil was changed by manipulating the values of the x and y components of the inlet velocity. Both lift and drag forces were calculated normal to, and along the inlet velocity vector direction, respectively. The lift and drag coefficients were calculated for each angle of attack using equations 3 and 4, respectively while pressure coefficient was calculated using equation 5.

$$C_l = \frac{2L}{\rho A V^2} \tag{3}$$

$$C_d = \frac{2D}{\rho A V^2} \tag{4}$$

$$C_p = \frac{P_s - P_\infty}{\frac{1}{2}\rho V^2} \tag{5}$$

where L and D represents the lift force and drag force, respectively, ρ is air density, A is airfoil planar area (equal to chord length C x 1), P_s is the surface pressure, P_∞ is the free stream pressure and V is the free stream velocity. In the present work, the airfoil has a chord length of 1 m while the air velocity magnitude is 7.1 m/s. The combination of chord length, air velocity and standard air density and viscosity result in Reynolds number, based on airfoil chord, of 500,000.

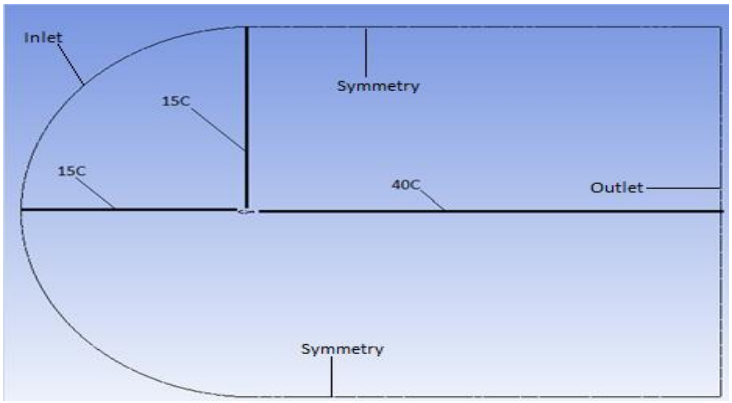

Fig. 2: The numerical solution domain and boundary conditions

© 2020, www.IJARIIT.com All Rights Reserved

Different numerical mesh parameters were examined, and a mesh independency test was done by observing the value of the computed lift coefficient at an angle of attack of 5 degrees. Figure 3 shows the adopted mesh shapes where unstructured mesh was used everywhere except near the airfoil surface where a structured mesh made of 40-80 inflation layers was used. The mesh distribution following the inflation layer was also refined to obtain accurate results

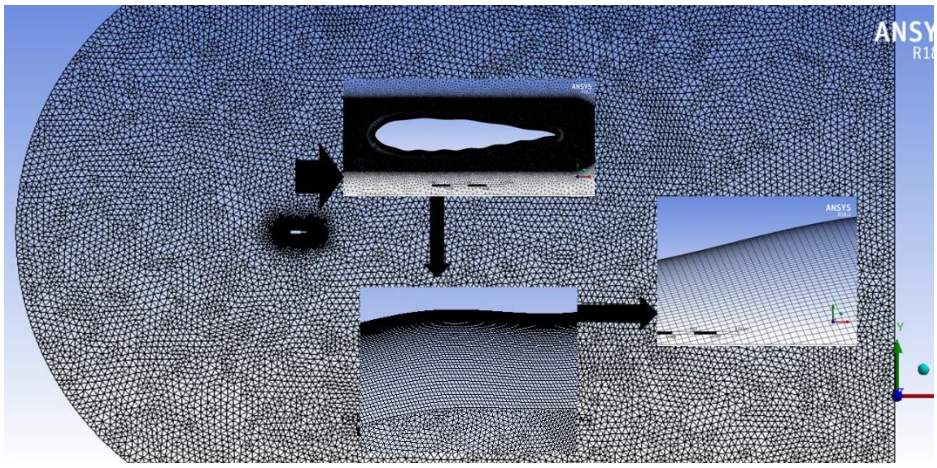

Fig. 3: The numerical solution mesh shape

Table 3 shows the obtained lift coefficient of the basic NACA 0018 airfoil at an angle of attack of 5 for different mesh sizes included in the mesh independency test. The computed lift coefficient varies from 0.45888 for mesh 1 to 0.4825 for mesh 4. The difference between the lift coefficient obtained by the coarse mesh and fine mesh (mesh 1 and mesh 4) is 5%. However, the difference between mesh 4 results and mesh 3 results is only 0.2%. Therefore, mesh 3 is adopted throughout the present work. Mesh 3 is shown in figure 3 below.

Table 3: Results of the mesh independency test

Mesh Parameter	Mesh 1	Mesh 2	Mesh 3	Mesh 4
No of nodes	210720	216879	226003	260402
inflation layers	40	60	70	80
Cl	0.45888	0.48143	0.48152	0.4825

Different turbulence models were investigated deeply in a study done by Balduzzi et al (2016). It was shown that the models which produce closest agreement with the experimental results of airfoils are the kω − SST model and the realizable kε model. The latter model offers good prediction of the near wall flow characteristics (Francesco Balduzzi, 2016). The kω − SST model can predict the near-wall flow more accurately but a finer mesh near the wall is needed. The realizable k − ε offers good prediction of free stream flows outside the boundary layer. In order to ensure that the present simulation are viable, the flow around the NACA0018 airfoil was performed in the present study using both turbulence models and the results were compared with experimental results obtained from the NASA experiment (Rumsey, 2017).

Fig. 4 shows the predicted variation of Cl with AoA for the NACA 0018 airfoil using both the kω − SST and the realizable kε turbulence models. Comparison with the experimental results, also included in Fig. 4, show that both models are in close agreement with the experiments for AoA varying from 0 to 14 degrees. Therefore, the realizable kε turbulence model is selected for further simulations.

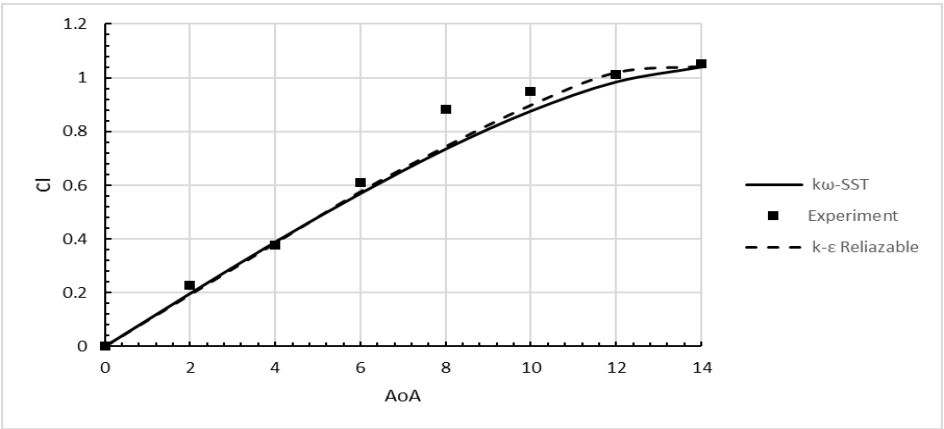

Figure 4: Computed variation of lift coefficient with angle of attack for NACA 0018 airfoil using different turbulence models, compared with experimental measurements by (Rumsey, 2017)

4. RESULTS AND DISCUSSION

4.1 Suction side modifications

The suction side is first investigated. Different wave amplitudes as function of chord length (A_b/C) are studied while the period as a function of chord length (T_b/C) was fixed to 25%C. Figure 5 shows the predicted drag coefficient with different amplitudes along

© 2020, www.IJARIIT.com All Rights Reserved

the suction surface. The suggested modification show improvement in terms of reduction of the drag coefficient. It is found that using an amplitude of 0.3%C causes the lowest drag coefficient. The reason behind the improvement can be attributed to the presence of valleys, the valleys cause a delay in the separation which in turn decrease the drag force on the airfoil. This is in line with the results reported by (Jacobs E. , 1932) (Jacobs E. , 1932) (C. Lyon, 1997) (Owens W. E., 2005). The effect of surface bumps in terms of reducing the drag coefficient is also in line with the findings of Asif et al (2018).

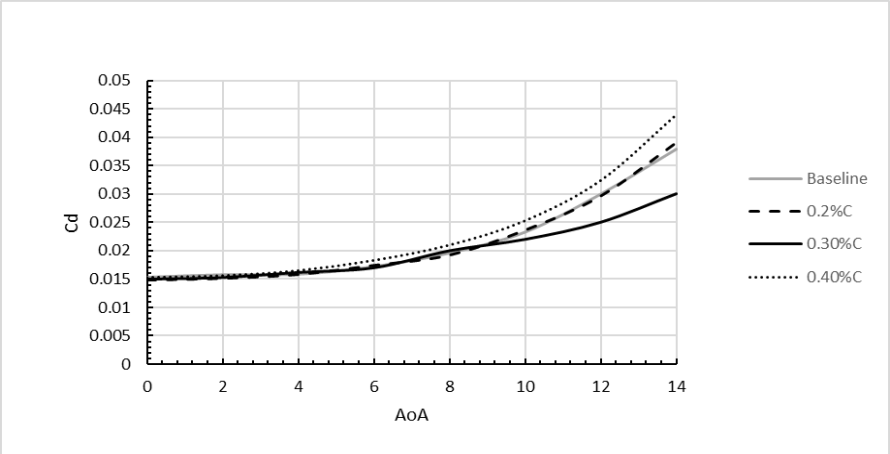

Fig. 5: Effect of suction surface bump amplitude on Cd - variation with AoA (Tb/C = 25%)

Investigating the lift force on the airfoil showed that the difference between the investigated geometries is moderate, Figure 6. The highest amplitude ratio of 0.4%C shows a lower lift coefficient than the baseline airfoil. The amplitude ratio of 0.3% shows slightly higher lift coefficient than the baseline airfoil at higher angles of attack.

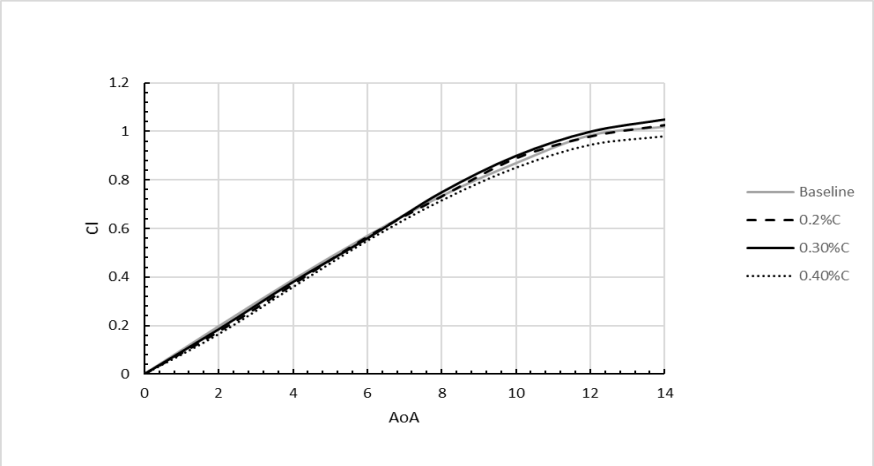

Fig. 6: Effect of suction surface bump amplitude on Cl - variation with AoA (Tb/C =25%)

Figure 7 shows the glide ratio variation with angle of attack for the different wave amplitudes. The baseline airfoil shows better performance at low angles of attack, this is because the separation in this range is minimal. Also, at these low angles of attack the lift force is relatively low and hence the implemented wave causes a drag penalty. As the angle of attack increases, the modified airfoil shows superior performance compared to the baseline airfoil, this is because the separation bubble starts to form on the top of the baseline airfoil. The modifications on the airfoil cause a delay in separation together with the reduction in the drag coefficient while lift coefficient remains relatively similar.

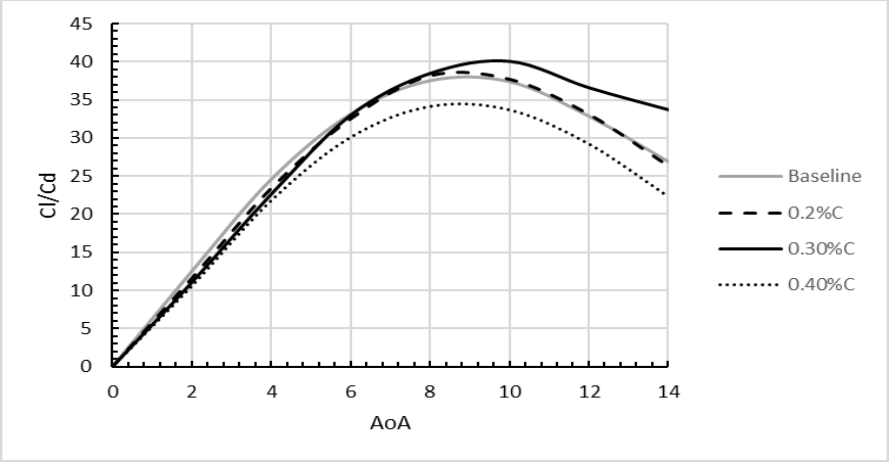

Fig. 7: Effect of suction surface bump amplitude on glide ratio - variation with AoA (Tb/C = 25%)

© 2020, www.IJARIIT.com All Rights Reserved

After studying the effect of changing the amplitude, the wave period is then studied. Amplitude to chord ratio (A_b/C) of 0.3% is kept constant as it showed the best aerodynamic performance. Wave periods, as a function of chord length (T_b /C) is varied. The investigated periods are 15%, 25% and 35%. Figure 8 shows the predicted drag coefficient for different wave periods at amplitude ratio of 0.3%. The difference in drag between the baseline airfoil and the modified airfoils with the highest period of 35%C is negligible. This might be because the high wave period offers very low changes to the surface and hence to the aerodynamic behavior of the airfoil. Decreasing the period to 25%C increases the number of waves on the surface and offers a better aerodynamic performance by decreasing the drag force. On the other hand, further reduction in the wave period to 15%C cause a slight increase in drag force. This can be attributed to the increase in surface roughness beyond the improvement limit and hence the drag increase.

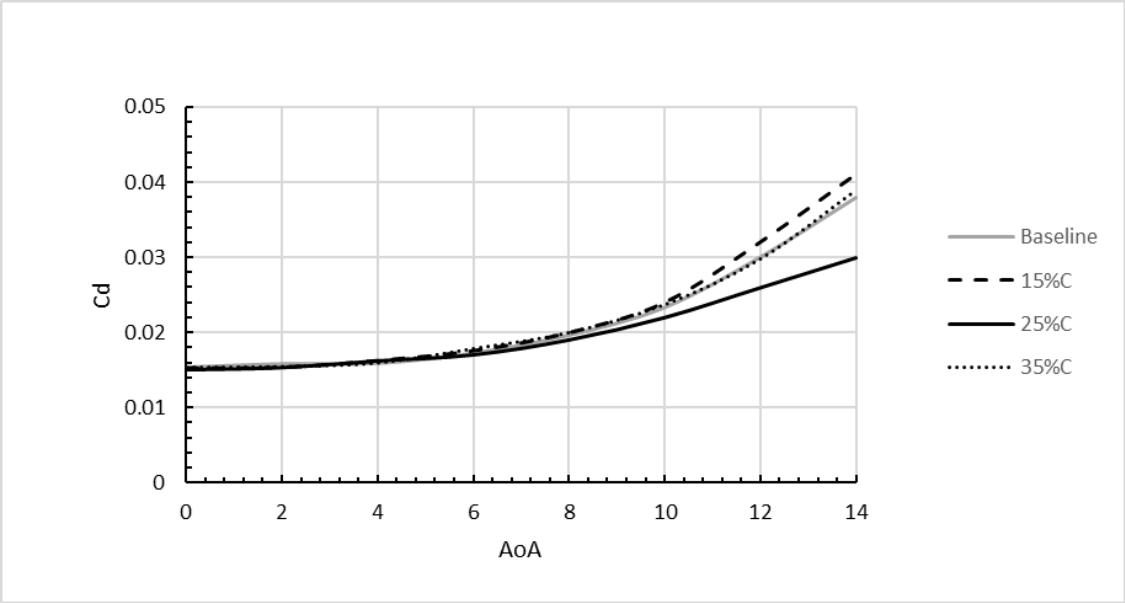

Fig. 8: Effect of suction surface bump wave period on Cd variation with AoA (A_b/C=0.3%)

The variation of lift coefficient with angle of attack at different wave periods is shown in Figure 9. It is shown that decreasing the period slightly increase the lift at higher angles of attack. The baseline airfoil, compared to the period of 35%C, shows almost no difference. On the other hand, wave lower periods show a slight increase of the lift coefficient. The highest lift is obtained for a period of 15%C. To accurately assess the aerodynamic behavior of the modifications glide ratio is used.

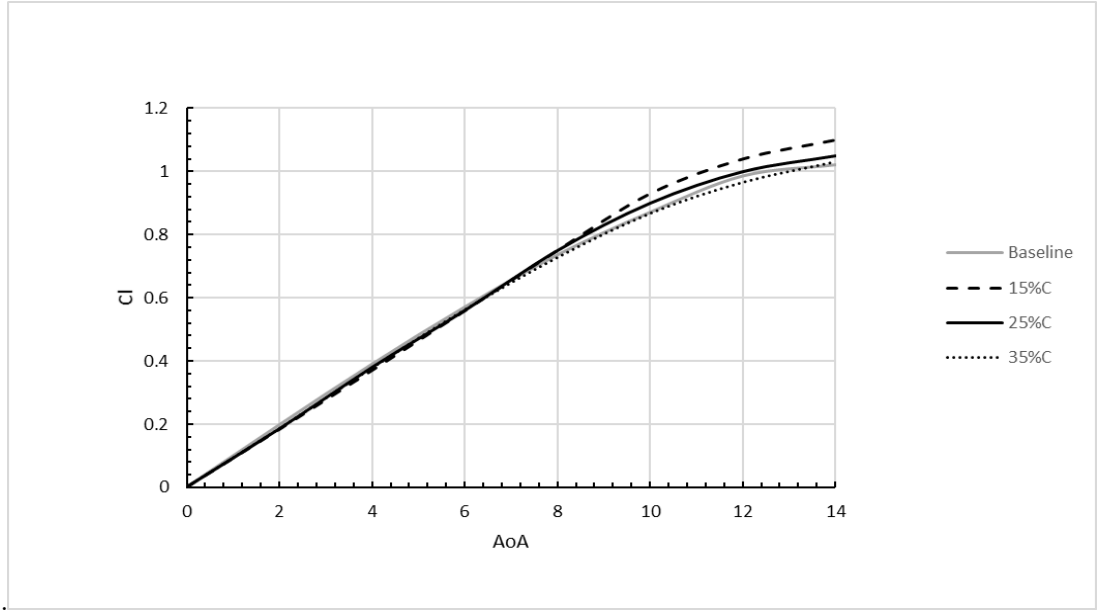

Fig. 9: Effect of suction surface bump wave period on Cl – variation with AoA (A_b/C=0.3%)

The investigation of glide ratio with the angle of attack for different wave periods is shown in figure 10. It is shown that for the largest wave period of 35%C the glide ratio is almost identical to the baseline airfoil. This is expected as both the lift and drag coefficients showed almost no difference. Reducing the period to 25%C shows an improvement of the glide ratio at higher angles of attack. This is also expected as the lift coefficient did not increase in a noticeable way but, on the other hand, the drag coefficient is much lower than that of the baseline airfoil. Alternately, the further reduction of the wave period to 15%C shows a slight decline of the glide ratio compared with the baseline airfoil. This is attributed to the much higher drag shown at this period. From this analysis it is concluded that the optimum configuration for the suction side wave is A_b/C=0.3 % and Tb/C = 25% which configuration 2 in table 1. The resulting airfoil shape for this configuration is shown in figure 11.

© 2020, www.IJARIIT.com All Rights Reserved

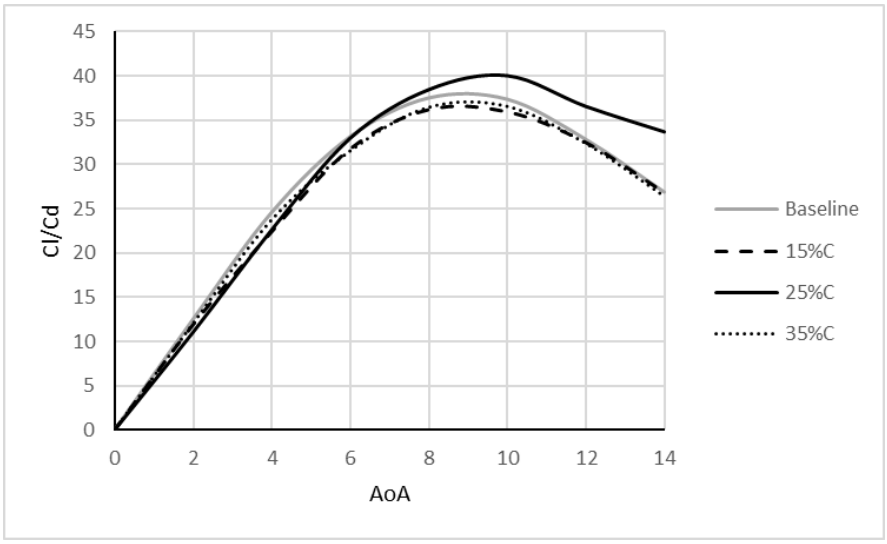

Fig. 10: Effect of suction surface bump wave period on glide ratio – variation with AoA (A_b/C=0.3%)

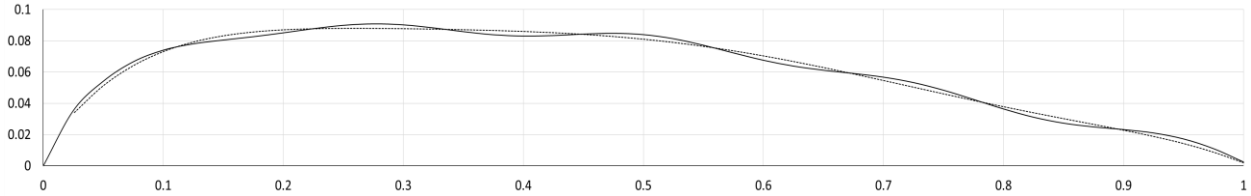

Fig. 11: Modified suction side of airfoil using a sine wave with A_b/C=0.3% and Tb/C = 25 %. Solid line: modified shape, dotted line: baseline airfoil

The flow characteristics are analyzed qualitatively using flow streamlines and velocity contours for the modified airfoil with the optimum configuration (A_b/C=0.3% and Tb/C = 25%) and angle of attack =14 degrees, as shown in Figure 12. It is clear that using surface bumps almost eliminates separation at this angle. This is in line with the findings in the lift and drag coefficients. At high angle of attack the delay in separation causes the drag reduction and hence the aerodynamic improvements shown in the glide ratio.

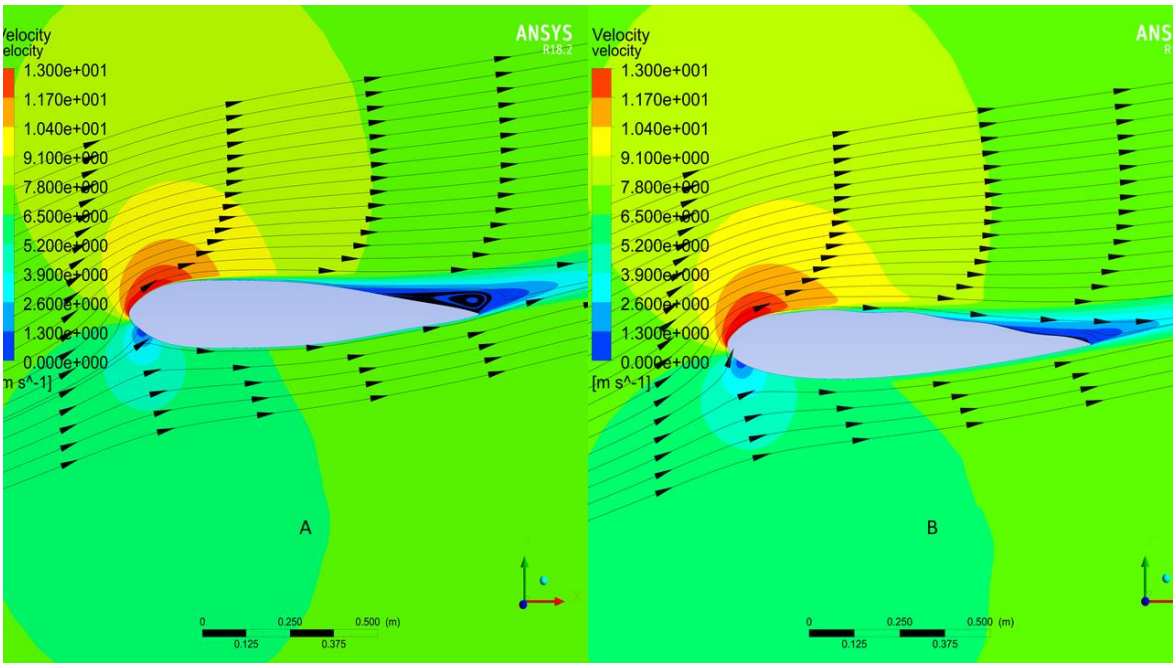

Fig. 12: Velocity contours and streamline for baseline airfoil (A) and modified suction side airfoil (A_b/C =0.3% and Tb/C = 25%) (B) at AoA = 14 deg.

4.2 Pressure side modifications

The same analysis methodology is used for the pressure side. The effect of changing the amplitude as a function of the chord length (A_b/C) is first investigated. The wave period (Tb/C) is fixed to 25%C throughout the investigation. Figure 13 shows the effect of changing the amplitude on the drag coefficient variation with angle of attack. As the wave amplitude increase the drag force on the airfoil increase, this might be attributed to the increase of the surface roughness. The decrease in drag phenomena that was found for the suction side bumps is not shown here. This is because the suction side bumps result in delay of separation while bumps introduced on the pressure side have no effect on separation.

© 2020, www.IJARIIT.com All Rights Reserved

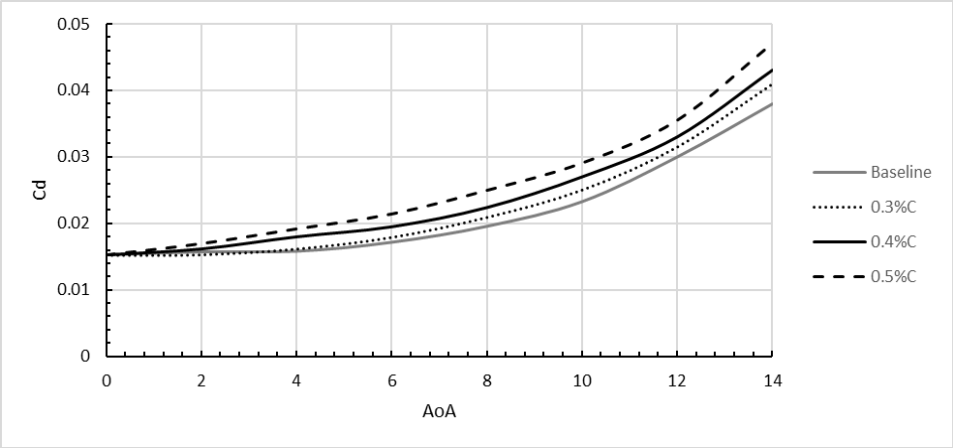

Fig. 13: Effect of Pressure surface bump amplitude on Cd variation with AoA (Tb/C = 25%)

Similarly, the increase in the lift force is found to be proportional to the wave bump. This is attributed to the entrapped flow in the lower bumps. The velocity of the air in the valley is lower than that on the surface. As per Bernoulli equation, the decrease in the velocity and hence the kinetic energy causes an increase in the pressure energy in the valleys. The increase in the pressure in the valley causes an increase in the pressure differential between the pressure and suction sides of the airfoil. Increasing the bump's amplitudes increases the air mass in the bump and hence increase the pressure inside the valley and increase the pressure differential causing higher lift. However, as the bump height increase from 0.4%C to 0.5%C the rate of lift increase is less than that between 0.3%C and 0.4%C. the variation of lift coefficient with angle of attacks is shown in figure 14.

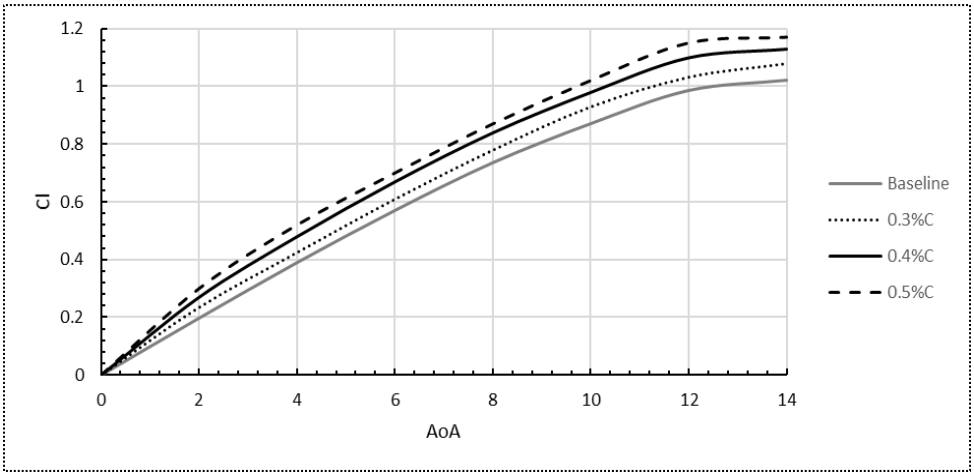

Fig. 14: Effect of pressure surface bump amplitude on Cl variation with AoA (Tb/C = 25%)

The rate of increase of lift and drag with the wave amplitude as a function of the chord is not constant. To accurately asses the ratio that offers the favorable aerodynamic performance of high lift and low drag glide ratio is investigated. As shown in figure 15, the lower surface bumps offer an improved performance. However, the amplitude to chord ratio of 0.4%C shows slightly higher glide ratio although the difference is minor.

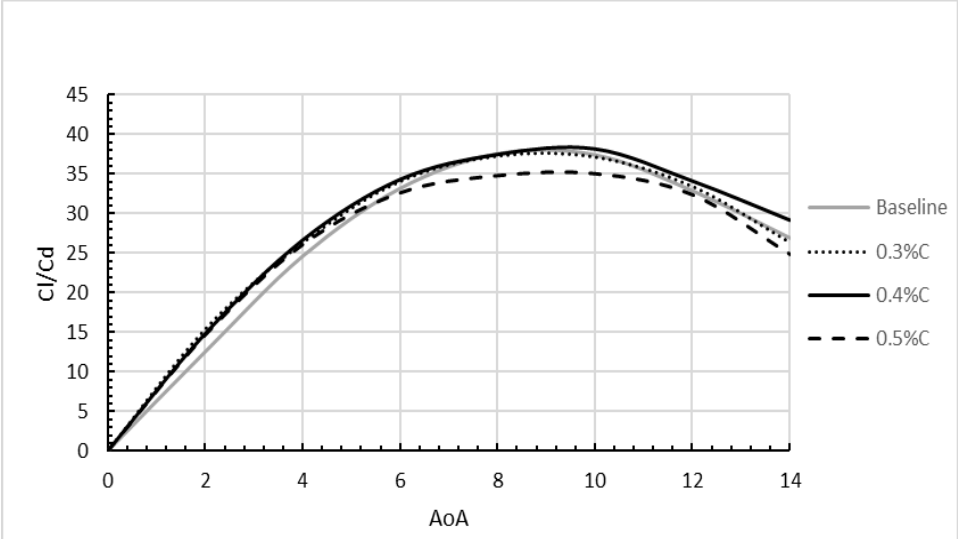

Fig. 18: Effect of pressure surface bump amplitude on glide ratio variation with AoA (Tb/C = 25%)

© 2020, www.IJARIIT.com All Rights Reserved

It is shown clearly that in the case of adding the sine wave to the pressure side the improvement is not only in the high angle of attack region, but improvement is also shown on the entire range of angles of attack. The optimum amplitude is found to be 0.4%C. the amplitude to chord ratio of 0.4% is then used to test different wave periods as a function of chord length to see their effect on the aerodynamic performance of the airfoil. As the wave period decrease the drag increase, this is due to the increase in surface roughness. This is shown in figure 16.

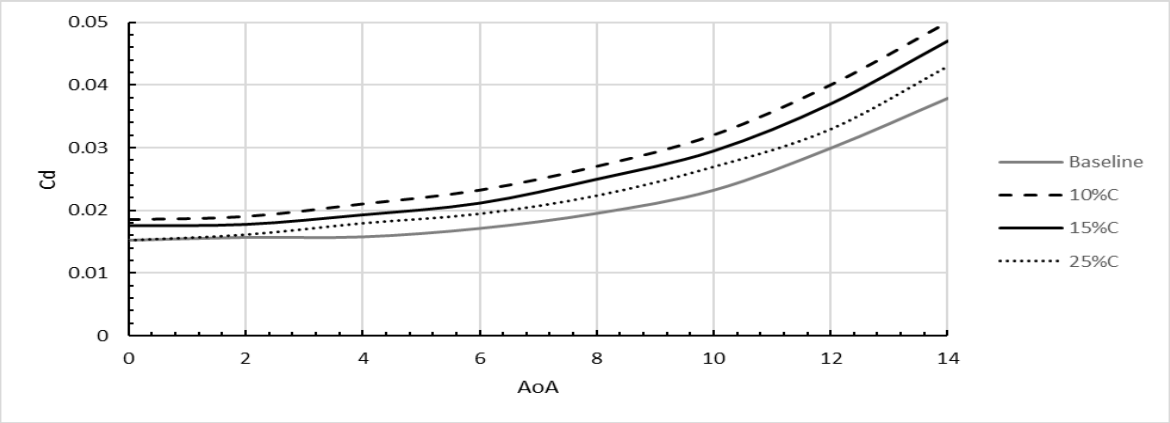

Fig. 16: Effect of pressure surface bump wave period on Cd – variation with AoA (A_b/C=0.4%)

As the wave period decrease the lift force increase, this is as a result of the increased numbers of valleys. However, as the period reaches a 0.1%C a decrease in the lift is observed. This decrease is attributed to the lower pressure zones at the peak. Reaching 0.1%C the improvement in the lift due to the presence of the valleys is opposed by the lower pressure zones at the peaks. The variation of lift coefficient with angle of attack is shown in figure 17.

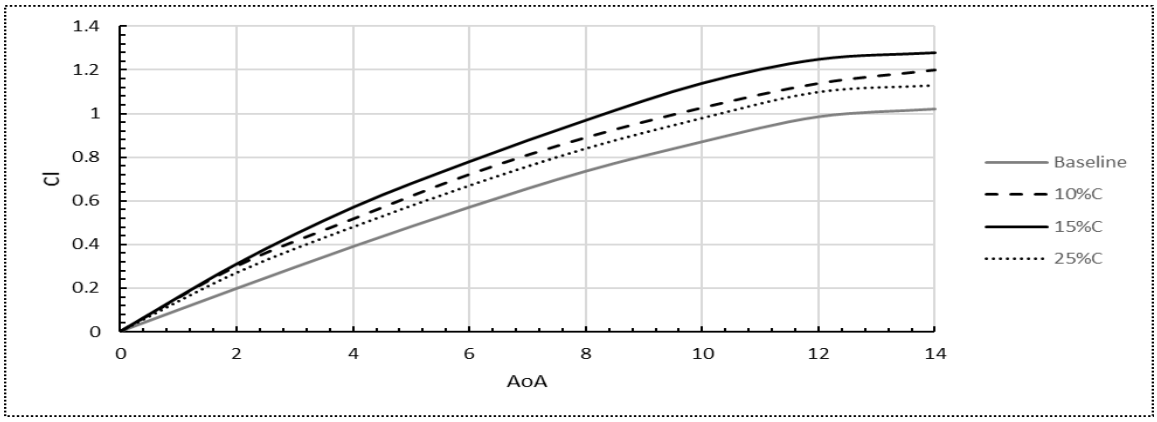

Fig. 17: Effect of pressure surface bump wave period on Cl – variation with AoA (A_b/C=0.4%)

It is clear that the introduction of surface bumps on the pressure side of the airfoil shows an improvement on the lift but on the other hand it also shows a drag penalty. Glide ratio variation with angle of attack is shown in figure 18. It is found that the increase in lift surplus the drag penalty and hence an improvement in the glide ratio is shown for a wave period of 0.15%C. However, as expected the higher period of 0.25%C showed almost minimum improvement as the increase in the lift force was not enough to overcome the associated drag penalty. The lowest wave period of 0.1%C showed a reduction in performance due to the drop-in lift compared to 0.15%C and at the same time increase in drag. The optimum configuration was hence found to be A_b/C=0.4% and Tb/C = 0.25%, this configuration is shown in figure 19.

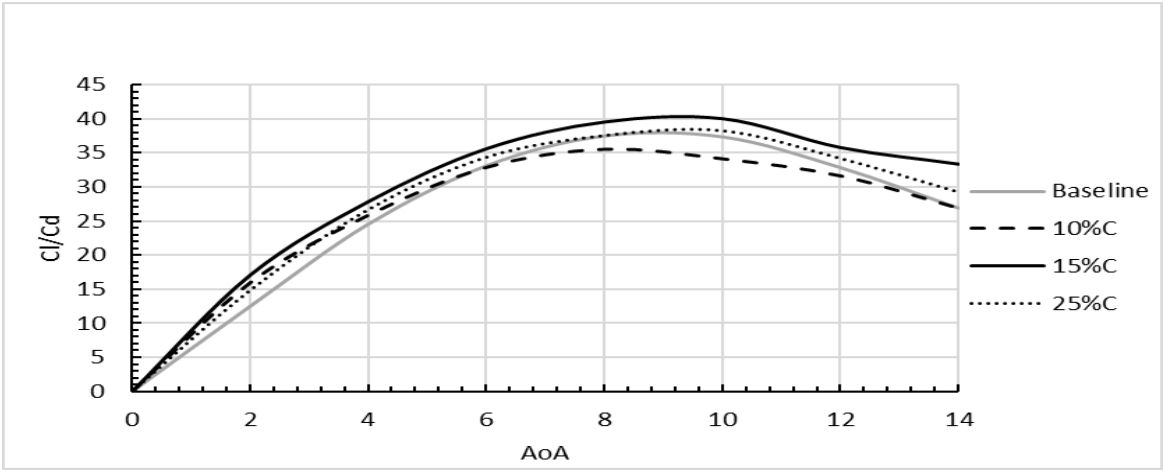

Fig. 18: Effect of suction surface bump wave period on glide ratio – variation with AoA (A_b/C=0.4%)

© 2020, www.IJARIIT.com All Rights Reserved

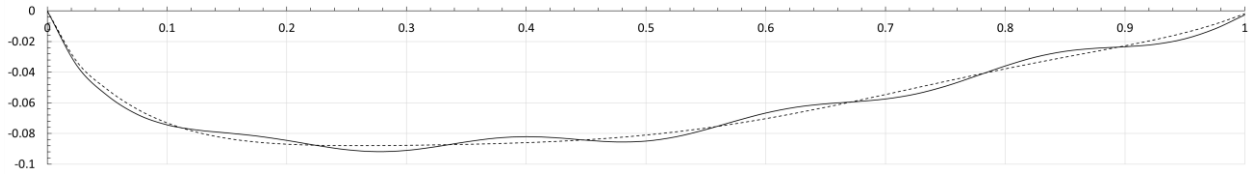

Fig. 19: Modified Pressure side airfoil A_b/C=0.4% and Tb/C = 15% - solid line modified shape while dotted line baseline airfoil

The improvement as a result of the lower surface modification took place as a result of the formation of high-pressure zones in the valleys. These high-pressure zones increase the differential pressure causing a higher lift force to be generated improving the performance. This is attributed to the lower velocity in the valleys as shown in the velocity contours in figure 20. Decreasing the period improved performance this might be due to the increase in the number of valleys and hence the areas of concentrated high pressure, this is visible in the pressure contours shown in figure 21. Further decreasing the period caused a drop in performance, this might be associated with the increase in drag force and the neutralization of the differential pressure increase by more regions of lower pressure at the peaks. The pressure side modification showed almost no impact on the flow separation as shown in the flow streamlines in figure 20.

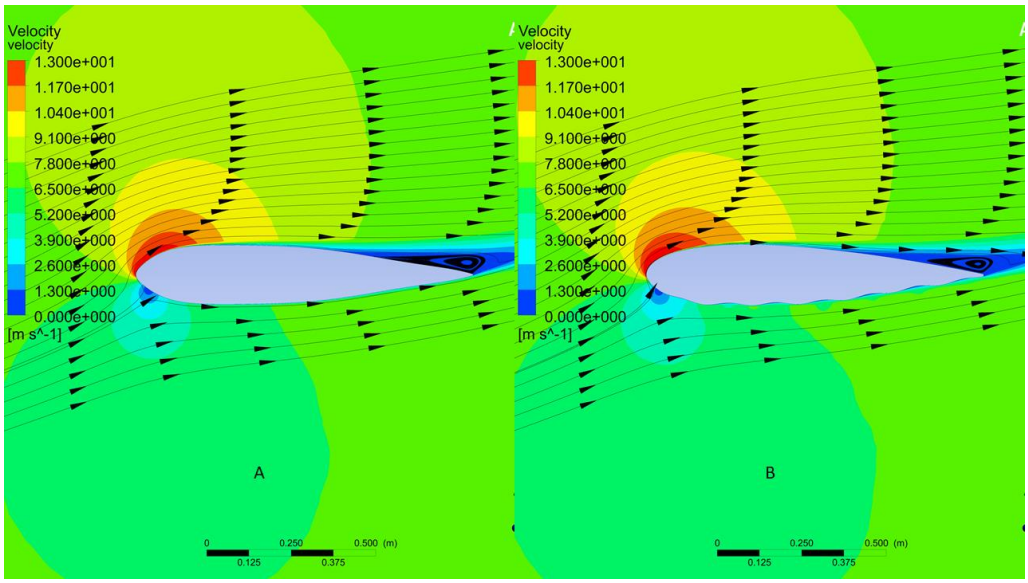

Fig. 20: Velocity contour and streamline for baseline airfoil (A) and modified pressure side airfoil (A_b/C =0.4% and Tb/C = 15%) (B) at AoA= 14 deg.

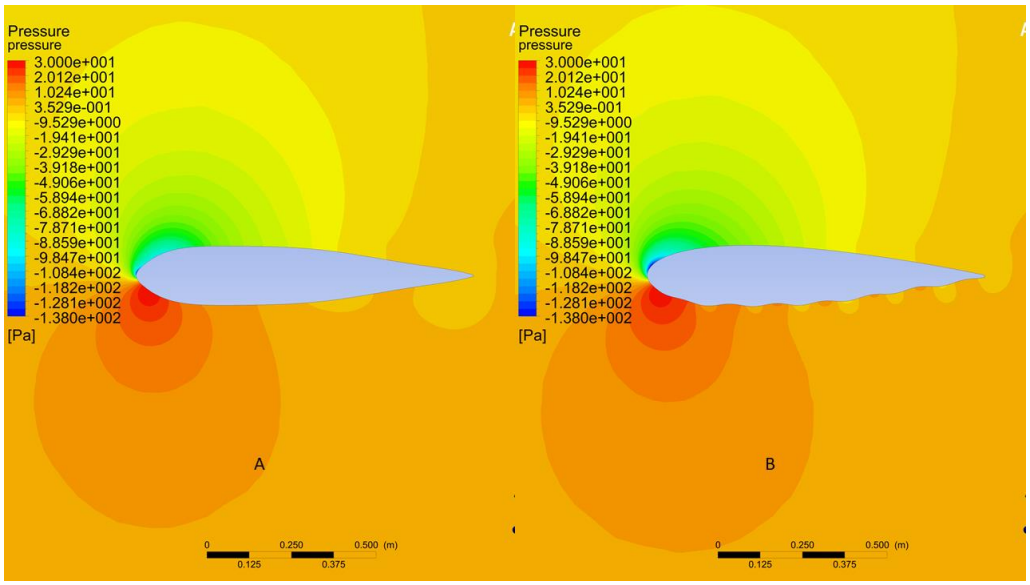

Fig. 21: Pressure contours for baseline airfoil (A) and modified pressure side airfoil (A_b/C =0.4% and Tb/C = 15%) (B) at AoA 14

4.3 Suction and Pressure side modifications combined

After evaluating each surface separately and finding the optimum period and amplitude, the two optimum configurations are joined together, this is shown in figure 22 where configuration of A_b/C =0.4% and Tb/C = 0.15 is adopted for the pressure side and configuration of A_b/C =0.3% and Tb/C = 0.25 is adopted for the suction side.

© 2020, www.IJARIIT.com All Rights Reserved

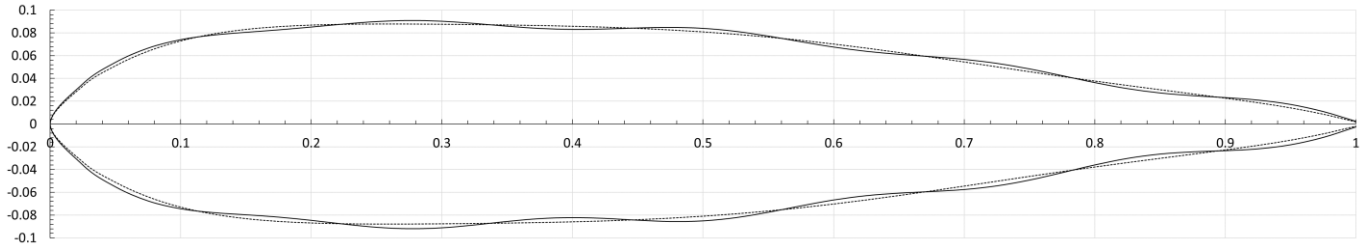

Fig. 22: Modified airfoil – pressure side (A_b/C=0.4%) and (Tb/C = 15%)- suction side (A_b/C=0.3%) and (Tb/C = 25%) - solid line modified shape while dotted line baseline airfoil

The drag coefficient for the modified airfoil is found to be higher than that of the baseline airfoil and lower than the high drag found in the modified pressure side airfoil. This behavior is because the modified airfoil is influenced by both the modifications on the suction side decreasing the drag and the pressure side which increases the drag. The variation of drag coefficient with angle of attack for the modified suction side airfoil, modified pressure side airfoil, baseline airfoil and completely modified airfoil is shown in figure 23.

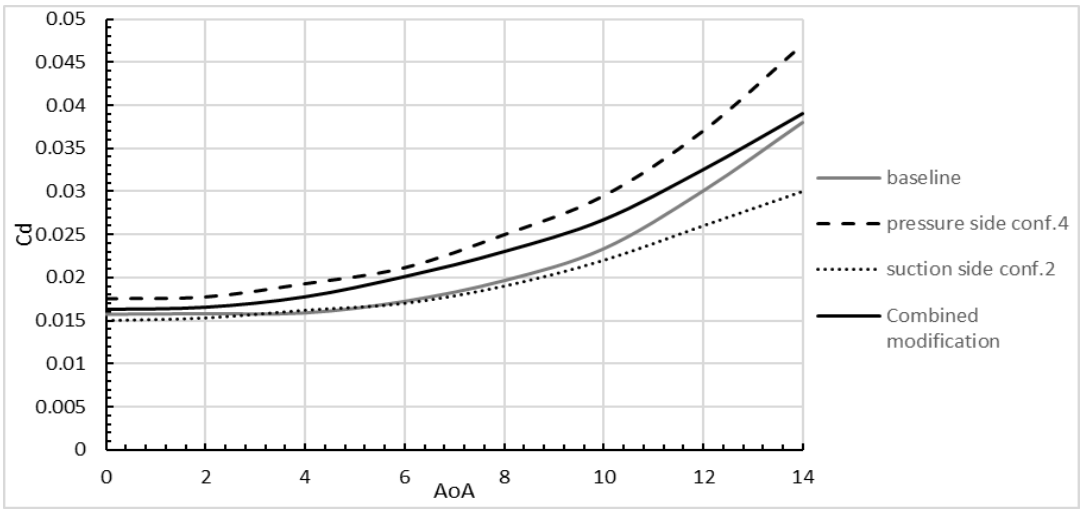

Fig. 23: Comparison between Cd for baseline, modified pressure side configuration 4, modified suction side configuration 2 and combined modification of airfoil – variation with AoA

The lift coefficient for the optimum configuration of the suction side, pressure side, modified airfoil and the baseline airfoil are compared in figure 24. The pressure side modification only shows an improvement in lift at angles of attack beyond 6 degrees, at lower angles of attack the lift is slightly lower than that of the baseline airfoil as it is not yet affected by separation. On the other hand, the pressure side modification showed a much higher lift coefficient when compared to the baseline airfoil through the entire range of angles of attack investigated. It is shown that the optimized airfoil shows higher lift than that found in the pressure side alone at angles of attack beyond 6 degrees. This is because the lower lift found on the pressure side alone at angles of attack below that contributes to the performance of the modified airfoil. At higher angles of attack the combined improvement from both surfaces is manifested in a higher lift for the modified airfoil. The higher lift found is also proved by analyzing the area governed by the pressure coefficient curve. The pressure coefficient curve shows the variation of pressure differential along the airfoil, the wavy shape observed in the curve is due to the presence of bumps on the airfoil surface. The area governed by the curve is clearly larger for the modified airfoil as shown in figure 25.

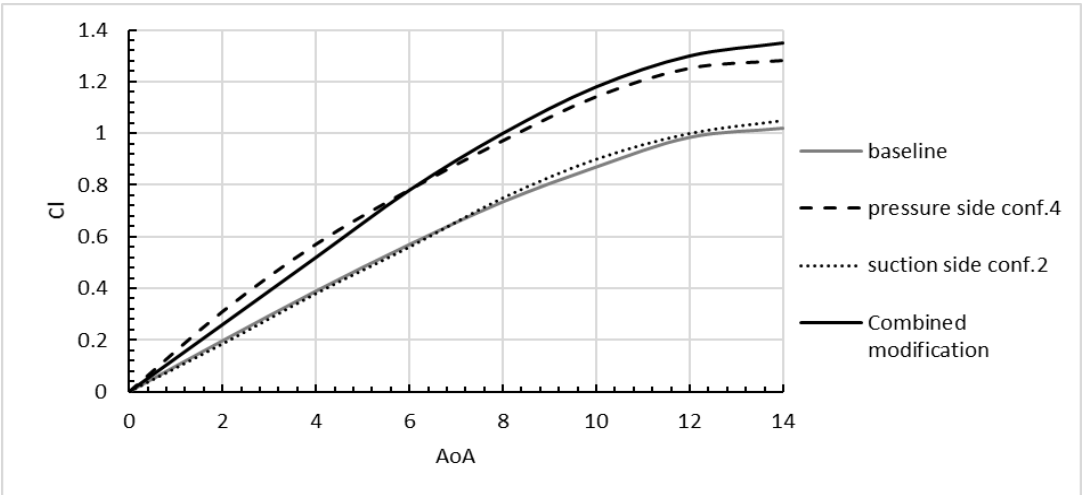

Fig. 24: Comparison between Cd for baseline, modified pressure side configuration 4, modified suction side configuration 2 and combined modification of airfoil – variation with AoA

© 2020, www.IJARIIT.com All Rights Reserved

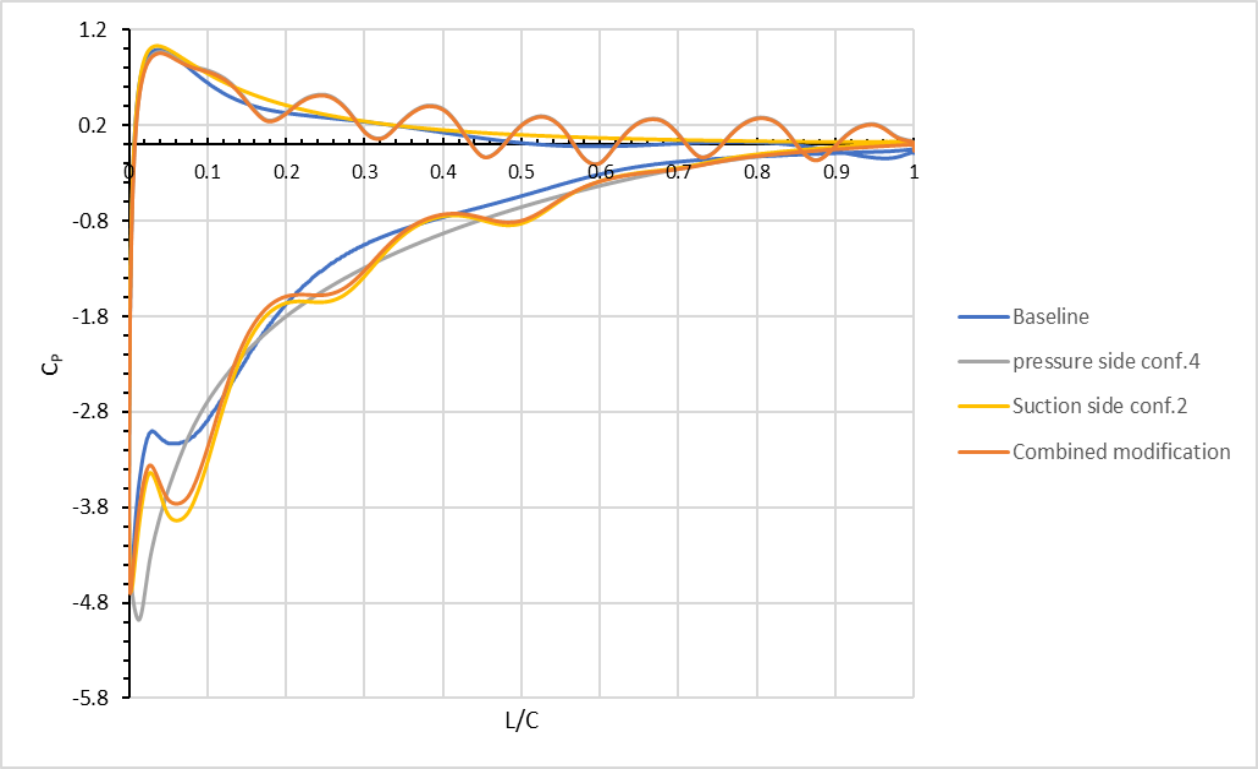

Fig. 25: Comparison between C_p for baseline, modified pressure side configuration 4, modified suction side configuration 2 and combined modification of airfoil – along airfoil surface

The glide ratio variation with angle of attack results for the optimum suction side, optimum pressure side, baseline and the modified airfoil is shown in figure 26. The fully optimized airfoil showed an enhanced performance benefiting from the improvement mechanisms found in both the suction side and pressure side modifications. The modified airfoil showed an aerodynamic performance that exceeded the pressure side modification after the angle of attack of 6 degrees. This is inline with findings from the lift and drag curves, the suction side show a slight increase in lift after the angle of attack exceed 6 degrees

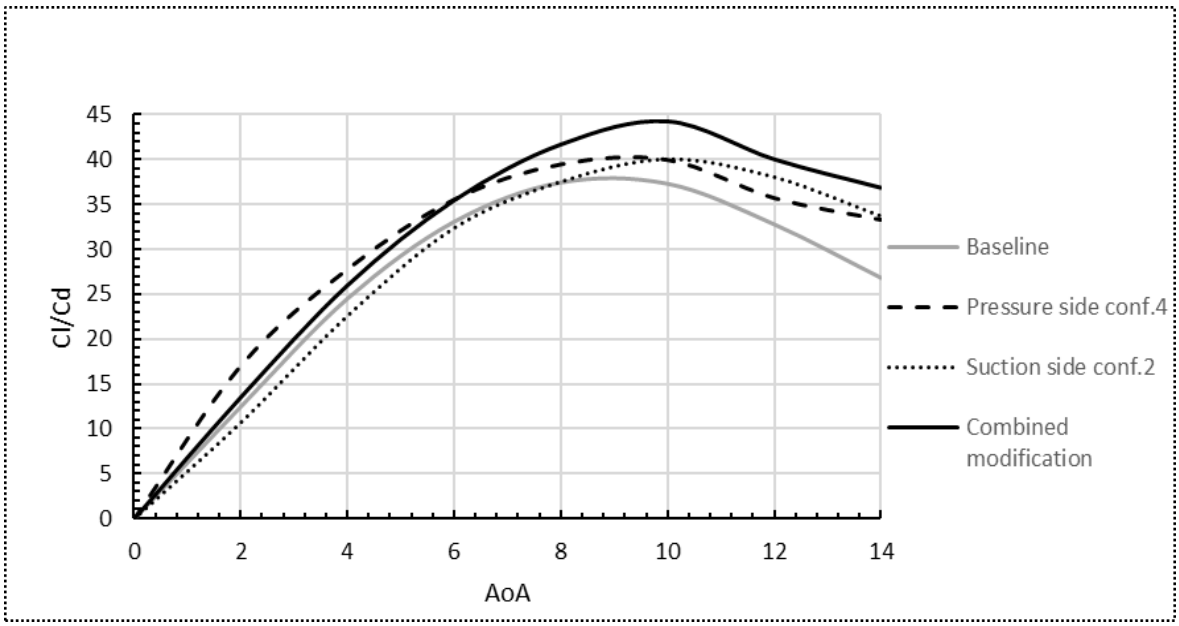

Fig. 26: Comparison between glide ratio for baseline, modified pressure side configuration 4, modified suction side configuration 2 and combined modification of airfoil – variation with AoA

The improvement shown for the modified airfoil benefiting from the modification of the suction side eliminating the separation and hence decreasing the drag, and the pressure side modification forming the high pressure spots and increasing the differential pressure and hence the lift force is also represented in the flow visualization shown in figures 27 and 28. The streamlines show the diminishing of the separation bubble on top of the modified airfoil (figure 27B), the separation bubble is seen on top of the baseline airfoil (figure 27A). The pressure contours in figure 28 clearly show the difference in pressure distribution on the airfoil surface. Figure 28B shows the high-pressure spots as a result of the pressure side modification.

© 2020, www.IJARIIT.com All Rights Reserved

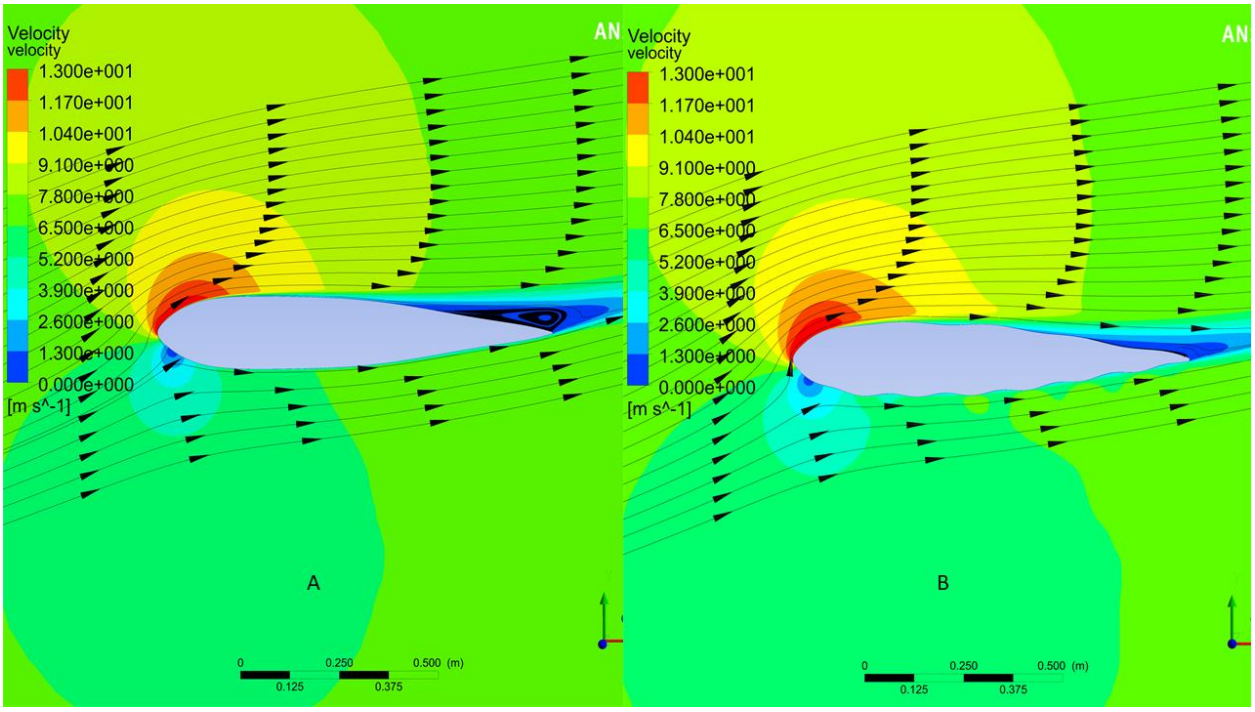

Fig. 27: Velocity contours and streamlines for baseline airfoil (A)and combined modification of airfoil [pressure side (A_b/C=0.4%) and (Tb/C = 15%),suction side (A_b/C=0.3%) and (Tb/C = 25%]) – AoA 14

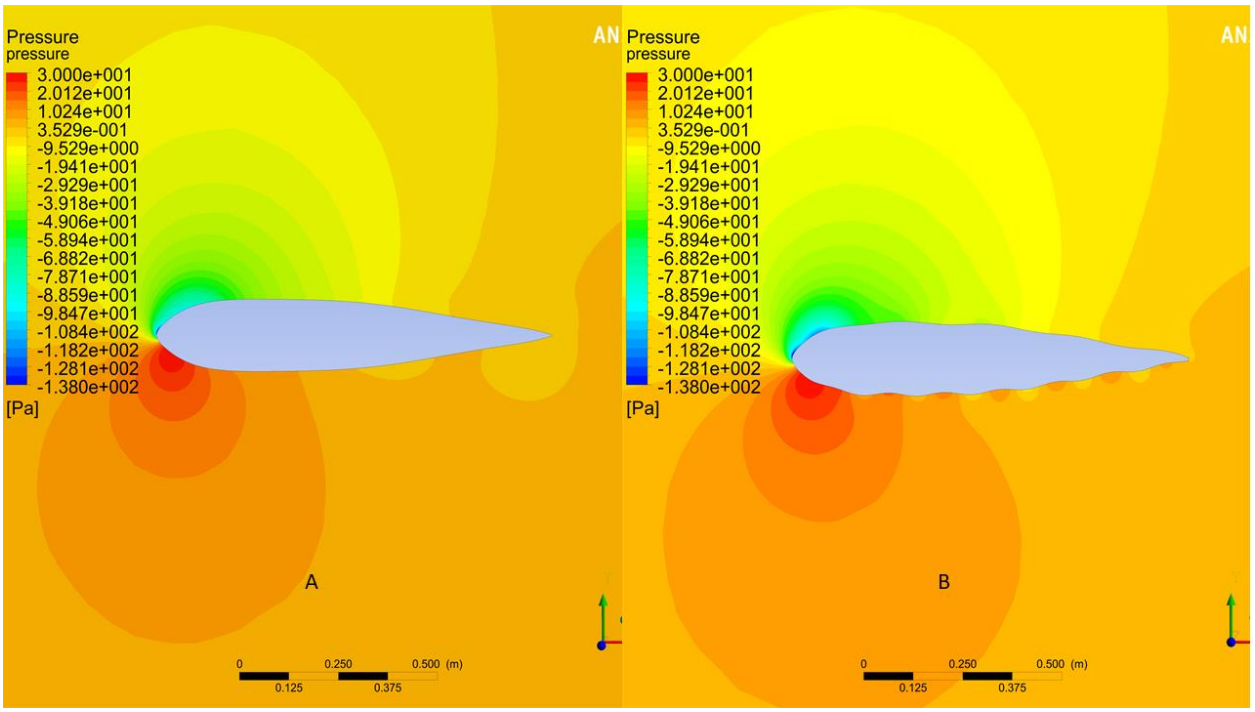

Fig. 28: Pressure contours for baseline airfoil (A)and combined modification of airfoil [pressure side (A_b/C=0.4%) and (Tb/C = 15%),suction side (A_b/C=0.3%) and (Tb/C = 25%]) – AoA 14

5. CONCLUSIONS

This study investigated the effect of using a bumpy surface inspired from hawk's wing on the aerodynamic performance of NACA0018 airfoil. Sine wave was used to introduce the bumps to the surface, this ensured smooth surface transition without abrupt changes. An approximate polynomial was used to represent the airfoil and the sine wave was then super positioned on it. The suction side and pressure side were studied independently. The parameters investigated were the wave amplitude as a function of the chord length (A_b/C) and the wave period (Tb/C) as a function of the chord length. The effect of changing these parameters was studied using numerical simulation methods. The lift, drag and pressure coefficients were obtained, and glide ratio was used to determine the optimum combination for each surface. The two optimum configurations were then combined forming a new shape of the airfoil. The findings of this study can be concluded in the following points:

- Introducing a wave with A_b/C = 0.3%C and Tb/C = 25%C to the suction side showed the best performance, this improvement was shown at angles of attack exceeding 8.
- The suction side improvement can be attributed to the elimination of separation which cause a slight increase in the lift force and a significant drop in drag

© 2020, www.IJARIIT.com All Rights Reserved

- Introducing a wave with A_b/C = 0.4%C and Tb/C = 15%C to the pressure side showed the best performance, the improvement is shown for the entire range of investigated angles of attack.
- The pressure side improvement can be attributed to the increase in lift. The lift increases due to the formation of high-pressure spots in the valleys. The pressure spots cause an increase in the pressure differential and hence higher lift force.
- The combined modification airfoil showed an increase in the glide ratio as a result of both modifications with a magnitude of approximately 17% compared to the clean baseline airfoil

6. REFERENCES

[1] Airfoil tools. (2020, 4 12). NACA-0018 coordinates: airfoil tools. Retrieved from airfoil tools : http://airfoiltools.com/airfoil/details?airfoil=naca0018-il#polars

[2] Asif Ali Laghari, Shafiq-ur-Rehman, M. Tarique Bhatti, Allah Rakhio, Manthar Ali Khoso and Sajjad Bhangwar. (2018). Role of single bump over the surface of E398 Airfoil to improve the aerodynamic performance. International Journal of Advance Research, Ideas and Innovations in Technology, 4(4), 550-556.

[3] B.G. Newman, S.B. Savage and D. Schouella (1977). Model test on a wing section of an Aeschna Dragonfly. Scale effects in animal loomotion, 445-477.

[4] C. Lyon, M. Selig, and A. Broeren. (1997). Boundary Layer Trips on Airfoils at Low Reynolds Numbers. 35th Aerospace Sciences Meeting & Exhibit. Reno.

[5] Dinesh Kumar G, Narmatha Pillai, K. Jithendra Sairam, Naveen S., Shajith F, B. Poovannan, Mona R. and Revathi (2014). Boundary Layer Supression Using Bump Surface in Airfoil. Journal of Basic and Applied Engineering Research, 7-12.

[6] E. van Nierop, S. Alben and M. P. Brenner. (2008). How Bumps on Whale Flippers Delay Stall: An Aerodynamic Model,. Physics Review Letters.

[7] F. E. Weick and J. A. Shortal. (1932). "The effect of multiple fixed slots and a trailing-edge flap on the lift and drag of a clark Y airfoil. NACA, Report No. 427, 531-536.

[8] Francesco Balduzzi, Alessandro Bianchini , Riccardo Maleci , Giovanni Ferrara and Lorenzo Ferrari (2016). Critical issues in the CFD simulation of Darrieus wind turbines. Renewable Energy , 419-435.

[9] Gasser E. Hassan, Amany Hassan and M. Elsayed Youssef. (2014). Numerical Investigation of Medium Range Re Number Aerodynamics Characteristics for NACA0018 Airfoil. CFD letters, 175-18

[10] H. Johari, C. Henoch, D. Cusodio and A. Levshin(2007). Effects of Leading-Edge Protuberances on Airfoil Performance, AIAA Journal, 2634-2642.

[11] Hamiltn and Tyler (2008). Whale-inspired wind turbines. MIT technology review.

[12] Jacob, Arvind Santhanakrishnan and Jame y D (2012). Effect of Regular Surface Perturbations on Flow Over an Airfoil. 35th AIAA Fluid Dynamics Conference and Exhibit. Toronto.

[13] Jacobs, E. (1932). Airfoil Section Characteristics as Affected by Protuberances. NACA TR-449.

[14] Jacobs, E. (1932). Wing Characteristics as Affected by Protuberances of Short Span. NACA T R–449.

[15] Y.P. Ju, C.H.Zhang (2012). Multi-point robust design optimization of wind turbine airfoil under geometric uncertainty, Journal of Power Energy, 226, 245-261.

[16] K. L. Hansen, R. M. Kelso and B. B. Dally, (2011). Performance Variations of Leading-Edge Tubercles for Distinct Airfoil Profiles. AIAA Journal, 185-194.

[17] A.B. Kessel,(2000). Aerodynamic characteristics of dragonfly wing section compared with technical airfoil. Journal of experimental biology, 3125-3135.

[18] M.Sun and G.Luo (2005). The effects of corrugations and wing planform on the aerodynamic force production of sweeping model insects wings. acta mech sinica, 531-541.

[19] McKee, Clarence L. Gillis and John W. (1941). "Wartime Report,". Natl. Advis. commitee Aeronaut.

[20] D.S.Miklosovic, (2004). Leading-edge tubercles delay stall on humpback whale (Megaptera novaeangliae) flippers. American Institute of physics.

[21] R.Mittal, Abel Vargas and Rajat (2004). Aerodynamic Performance of Biological Airfoils. Portland: AIAA- 2nd Flow Control Conference.

[22] Owens, William E. Milholen II and Lewis R. (2005). On the Application of Contour Bumps for Transonic Drag Reduction. AIAA Journal , 23681-2199.

[23] R.Mittal and M.Kwok (2005). Experimental investigation of the aerodynamics of a modeled dragonfly wing section. AIAA-region I-MA student conference. Verginia .

[24] C.J.C .Rees (1975). Aerodynamc properties of an insect wing section and a smooth airfoil compared. Nature, 141-142.

[25] Rumsey, Christopher A. Eggert and Christopher L. (2017). CFD Study of NACA 0018 Airfoil with Flow Control. Verginia : NASA.

[26] M.J. Stanway (2008). Hydrodynamic effects of Leading-Edge tubercles on control surfaces and in flapping foil propulsion. Massachuetus: MIT-Msc. Thesis .

[27] T. H. New, Y. X. Chan, G. C. Koh, M. C. Hoang and Shengxian Shi (2014). Effects of corrugated aerofoil surface features on flow separation control. AIAA Journal.

[28] Tze Pei Chong, Alexandros Vathylakis, Archie McEwen, Foster Kemsley, Chioma Muhammad and Saarim Siddiqi (2015). Aeroacoustic and Aerodynamic Performances of an Aerofoil Subjected to Sinusoidal Leading Edges. Dallas : 21st AIAA/CEAS Aeroacoustics Conference.

[29] Zilong Zhang, Yajun Yin, Zheng Zhong and Hongxiao Zhao. (2015). Aerodynamic Performnce of Dragonfly wing with Well Designed Corrugated section in Gliding Flight. CMES, 285-302.

© 2020, www.IJARIIT.com All Rights Reserved